THE JOURNAL OF PHYSICAL CHEMISTRY B

Article

Pivotal Role of Water in Terminating Enzymatic Function: A Density Functional Theory Study of the Mechanism-based Inactivation of Cytochromes P450

Hajime Hirao, Zhi Hao Cheong, and Xiaoqing Wang

J. Phys. Chem. B, **Just Accepted Manuscript** • DOI: 10.1021/jp302592d • Publication Date (Web): 23 May 2012

Pivotal Role of Water in Terminating Enzymatic Function: A Density Functional Theory Study of the Mechanism-based Inactivation of Cytochromes P450

Hajime Hirao,* Zhi Hao Cheong, Xiaoqing Wang

Division of Chemistry and Biological Chemistry, School of Physical and Mathematical Sciences,

Nanyang Technological University, 21 Nanyang Link, Singapore 637371

* Corresponding authors. E-mail: hirao@ntu.edu.sg

Abstract

The importance of the mechanism-based inactivation (MBI) of enzymes, which has a variety of physiological effects and therapeutic implications, has been garnering appreciation. Density functional theory calculations were undertaken to gain a clear understanding of the MBI of a cytochrome P450 enzyme (CYP2B4) by *tert*-butylphenylacetylene (tBPA). The results of calculations suggest that, in accordance with previous proposals, the reaction proceeds via a ketene-type metabolic intermediate. Once an oxoiron(IV) porphyryn π-cation radical intermediate (compound I) of P450 is generated at the heme reaction site, ketene formation is facile, as the terminal acetylene of tBPA can form a C–O bond with the oxo unit of Cpd I with a relatively low reaction barrier (14.1 kcal/mol). Unexpectedly, it was found that the ketene-type intermediate was not very reactive. Its reaction with the hydroxyl group of a threonine (Thr302) to form an ester bond required a substantial barrier (38.2 kcal/mol). The high barrier disfavored the mechanism by which these species react directly. However, the introduction of a water molecule in the reaction center led to its active participation in the reaction. The water was capable of donating its proton to the tBPA substrate, while accepting the proton of threonine. This water-mediated mechanism lowered the reaction barrier for the formation of an ester bond by about 20 kcal/mol. Therefore, our study suggests that a water molecule, which can easily gain access to the threonine residue through the proton-relay channel, plays a critical role in enhancing the covalent modification of threonine by terminal acetylene compounds. Another type of MBI by acetylenes, N-alkylation of the heme prosthetic group, was less favorable than the threonine modification pathway.

1. Introduction

The formation of irreversible, covalent adducts in the active sites of enzymes via the so-called mechanism-based (or suicide) inactivation (MBI) has a variety of physiological effects and therapeutic implications.[1] This covalent modification is observed relatively frequently in animal cytochrome P450 (P450) enzymes,[2-7] heme enzymes essential for the metabolism of xenobiotics including drugs. The beneficial effects of the MBI of P450 include the possibility of achieving a high degree of selectivity when a specific P450 is selected as a drug target.[2,3] This potentially high selectivity arises from the fact that covalent adducts are formed only after compounds are catalytically transformed into reactive metabolic intermediates, i.e., compounds must have substrate-like structures to fit into the enzyme's active site. Mechanism-based inactivators have played important roles in the study of P450s, such as the identification of active-site amino acid residues, elucidation of P450 reaction mechanisms, and determination of the specific P450s that are responsible for the catalysis of a particular reaction.[3] The downside of MBI is that it could impair the essential metabolic function of P450, potentially resulting in adverse drug-drug interactions or toxicity.[8,9] P450 enzymes that have only low substrate specificity, as in CYP3A4, may be susceptible to MBI by a variety of drugs. In such cases, a precise understanding of MBI is of critical importance because the pharmacokinetics of drugs can be greatly influenced by MBI. All these factors render the molecular understanding of MBI an important research goal; however, the X-ray crystal structures of a P450 bound to a mechanism-based inactivator have been solved only recently.[10a]

There are several types of P450 MBI.[2] Among them, acetylene compounds form a covalent bond with an active-site threonine residue to act as mechanism-based inactivators of many animal P450s including CYP1A1, 1A2, 2A1, 2A6, 2B1, 2B4, 2B5, 2B6, 2B11, 2C2, 2C14, 2E1, 3A4, and 3A5.[10-13] Experimental data indicate that MBI by terminal acetylenes involves the formation of a

reactive ketene intermediate (Scheme 1).[11] A mass shift observed in electrospray ion trap mass spectrometry was consistent with the generation of a ketene in the reaction.[11b] *tert*-Butylphenylacetylene (tBPA) inhibits several CYP2B enzymes in a mechanism-based fashion. For example, CYP2B4 is inhibited by tBPA. In a recent paper, Gay et al. reported the X-ray crystal structures of CYP2B4 that was covalently bound to tBPA.[10a] In the X-ray structures, tBPA was bound to a threonine residue (Thr302) located in the active site of P450. P450 enzymes commonly possess this threonine residue (although perhaps with a somewhat different residue number), which acts as a catalytically essential residue. It is widely believed that a proton is relayed using water molecules from a carboxylate side chain via the threonine to the distal oxygen of the ferric–hydroperoxy species of P450, the so-called compound 0 (Cpd 0).[13,14] As a result, compound I (Cpd I) is generated, which acts as a reactive species to activate the inert C–H bonds of substrates (Scheme 1). The potential consequences of the covalent modification of the threonine residue are interruption of the proton relay and permanent occupation of the active site by the covalent adduct, both of which possibly interfere with the catalytic cycle of the enzyme (Scheme 1). The interesting phenomenon of MBI, especially the MBI of CYP2B4 by tBPA, was the focus of this computational study, which was performed using density functional theory (DFT) calculations.

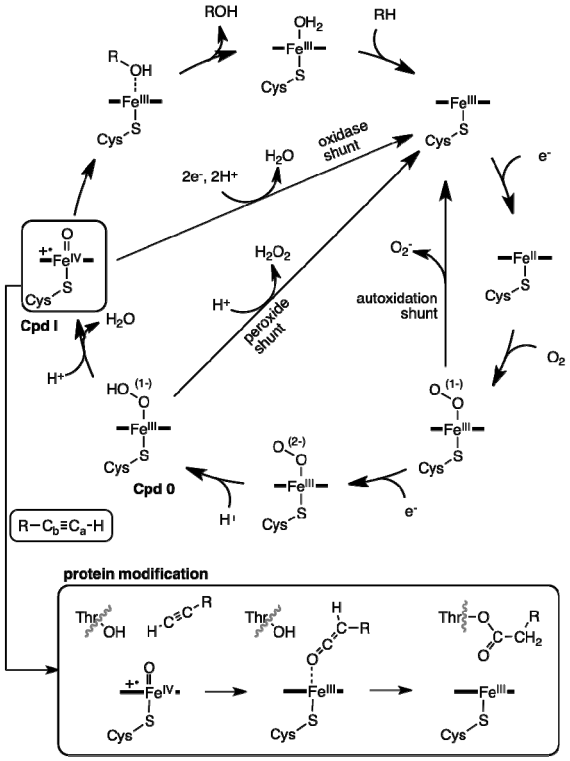

Scheme 1. Catalytic cycle of P450 (top)[13] and likely mechanism of protein modification via mechanism-based inactivation by terminal acetylenes (bottom).

Over the last decade or so, the reaction mechanisms of P450s have been an attractive research subject in the field of computational chemistry.[14-19] Studies using DFT and DFT/MM (i.e., joint DFT and molecular mechanics) methods have derived fundamental insights into the patterns of P450 reactions. The C–H hydroxylation and C=C epoxidation reactions have been particularly well studied. In comparison, the oxidation of C–C triple bonds by P450s, which has significant implications for MBI, remains to be studied in depth. This also prompted us to perform computational studies of the reaction between tBPA and a P450 model, using DFT calculations.

2. Method

All DFT calculations were performed using the Gaussian 09 program.[20] Based on the

consensus mechanism of P450 catalysis (Scheme 1), we assumed that Cpd I is the reactive species for the reaction with the terminal acetylene of tBPA. The doublet, quartet, and sextet spin states of Cpd I were considered. To make calculations of the enzymatic system feasible, we employed truncated models of heme and threonine (Scheme 2). A porphine ligand was used to model the porphyrin ligand of P450, and the cysteinate ligand was replaced with HS^-. In the final stage of the reaction, a ketene intermediate and Thr302 undergo a reaction with each other (Scheme 1). To dissect this process, ethanol (CH_3CH_2OH) was used to model the threonine. As we shall discuss in the text, a water molecule appeared to play a critical role in this final step of the reaction. Therefore, a water molecule was also included in the calculation for one of the paths considered. However, unlike a real protein, the steric restraint that holds the threonine residue and a water molecule at a specific position was missing in this truncated model. Therefore, the threonine model and a water molecule were added to the reaction after the ketene intermediate was obtained. Geometry optimization calculations were performed at the B3LYP/[SDD(Fe),6-31G*(others)] level of theory, and subsequently, optimized geometries were subjected to single-point calculations at the B3LYP/6-311+G(d,p) level in the gas phase and with the solvent effect included using the SCRF(IEFPCM) model.[21-23] The [SDD(Fe),6-31G*(others)] and 6-311+G(d,p) basis sets are, henthforce, referred to as B1 and B2, respectively. The B3LYP functional is known the reproduce the spin-state ordering of P450 systems reasonably well.[14] A dielectric constant value of 5.7 was used for SCRF calculations to mimic the polar environment in the enzyme.[24] Vibrational calculations were performed at the B3LYP/B1 level, and the energies reported herein are B3LYP(SCRF)/B2//B3LYP/B1 values that include the zero-point energy effect evaluated using B3LYP/B1. UCSF Chimera was used for molecular visualization.[25] Key data are presented in the paper, whereas other data are described in the Supporting Information (SI).

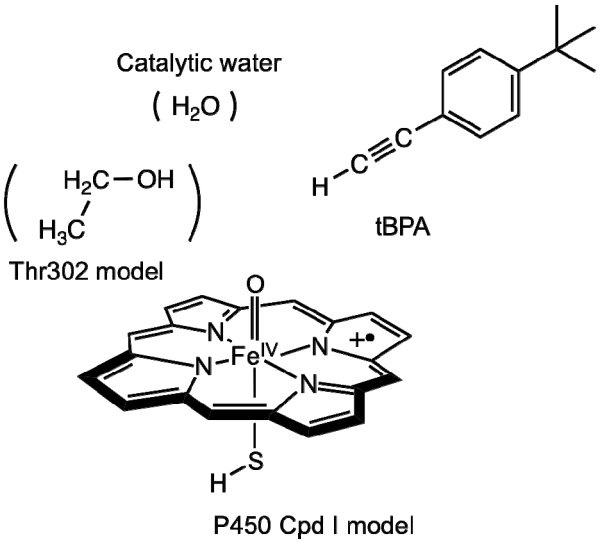

Scheme 2. Model used in our computational study. The groups in parentheses were added in the late stage of the reaction.

3. Results and Discussion

3.1. Formation of a ketene-type metabolic intermediate

A pathway has been proposed for the formation of ketene in the MBI reaction process (Scheme 1). However, as far as we are aware, no computational study of this process has been performed. To examine the feasibility of ketene formation, we performed a series of DFT calculations. The calculated reaction energy profile is shown in Figure 1 and the optimized geometries for key species are summarized in Figure 2. In the reaction considered here, Cpd I and tBPA initially form a weakly bound reactant complex (**RC**, Figure 2a), with the terminal hydrogen pointing to and interacting with the oxo moiety of Cpd I. At this stage, the doublet and quartet states are virtually degenerate, whereas the sextet state is higher in energy by > 10 kcal/mol (Figure 1). Subsequently, the terminal acetylene carbon approaches the oxo moiety to form a new C–O bond via a transition state, $\mathbf{TS_{co}}$. The activation barriers for this step are 14.1 (doublet) and 15.8 (quartet) kcal/mol, and the C–O distances at $\mathbf{TS_{co}}$ are 2.06 (doublet) and 2.01 (quartet) Å (Figure 2b). These relatively low barriers indicate that the initial C–O bond formation is rather facile. Spin density analysis shows that at $\mathbf{TS_{co}}$,

the tBPA substrate possesses a partial radical character, with the magnitudes of the B3LYP/B1-calculated spin density values for the substrate ranging between 0.22 and 0.33 (Table S4 in SI). In addition, the porphyrin-SH moiety, which has around one unpaired electron at **RC** retains some radical character at $\mathbf{TS_{co}}$. These results demonstrate that less than one electron has shifted to the Cpd I moiety at the transition state for C–O bond formation. Interestingly, the relative energy of the sextet state at $\mathbf{TS_{co}}$ was not as high as it was in the **RC** state: it was only < 6 kcal/mol higher than $^{2}\mathbf{TS_{co}}$ and $^{4}\mathbf{TS_{co}}$ (Figure 1). Thus, the sextet state became increasingly stable as the reaction progressed. A similar trend was observed previously for C–H hydroxylation and C=C epoxidation by P450 Cpd I.[16] The reaction in the sextet is accompanied by a shift of an electron from the substrate to the unoccupied d_{z2}-type molecular orbital of Cpd I, which results in enhanced exchange stabilization. The sextet state becomes more stable as the reaction progresses because of this exchange effect at the iron site.[16] As the d_{z2}-type molecular orbital is antibonding with respect to the Fe–S atom pair, electron occupation of this orbital resulted in an elongation of the Fe–S bond (Figure 2b). At the **Int1** stage, which is formed upon completion of C–O bond formation, the sextet state was as stable as the other two states. One can observe that the C–O bond is short (~1.25 Å) at **Int1** (Figure 2c), which is indicative of a partial double-bond character of this bond. In the doublet state, tracing the reaction path using the intrinsic reaction coordinate (IRC) method[26] led to $\mathbf{Int1_{rad}}$, in which only one electron had shifted from tBPA to Cpd I. However, a two-electron transferred intermediate state, **Int1**, was more stable than $\mathbf{Int1_{rad}}$ by 11.3 kcal/mol in the doublet state, indicating that the initial C–O bond formation actually results in a two-electron transferred intermediate. In the quartet and sextet spin states, **Int1** was directly obtained after $\mathbf{TS_{co}}$.

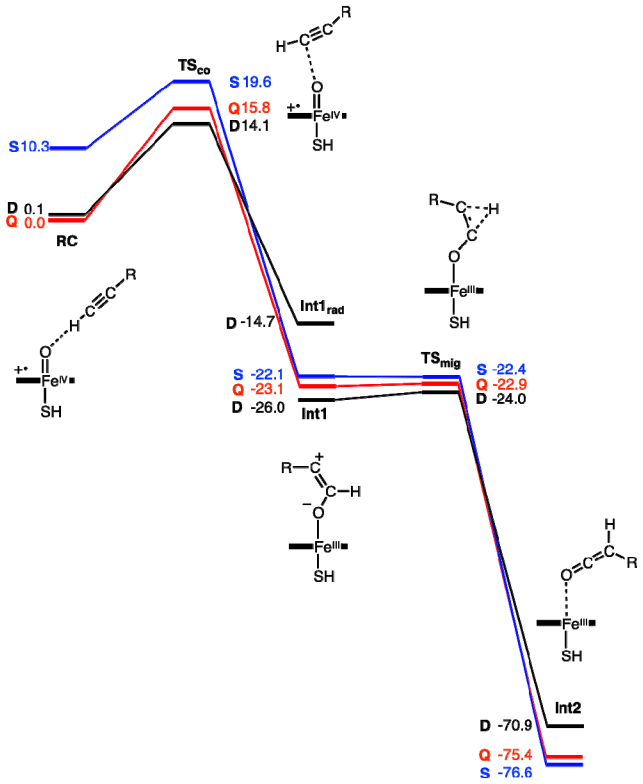

Figure 1. Reaction energy profiles for the formation of the ketene, as obtained at the B3LYP(SCRF)/B2//B3LYP/B1+ZPE(B1) level. The black, red and blue lines indicate the energy changes for the doublet (**D**), quartet (**Q**), and sextet (**S**) states, respectively. Relative energies are given in kcal/mol.

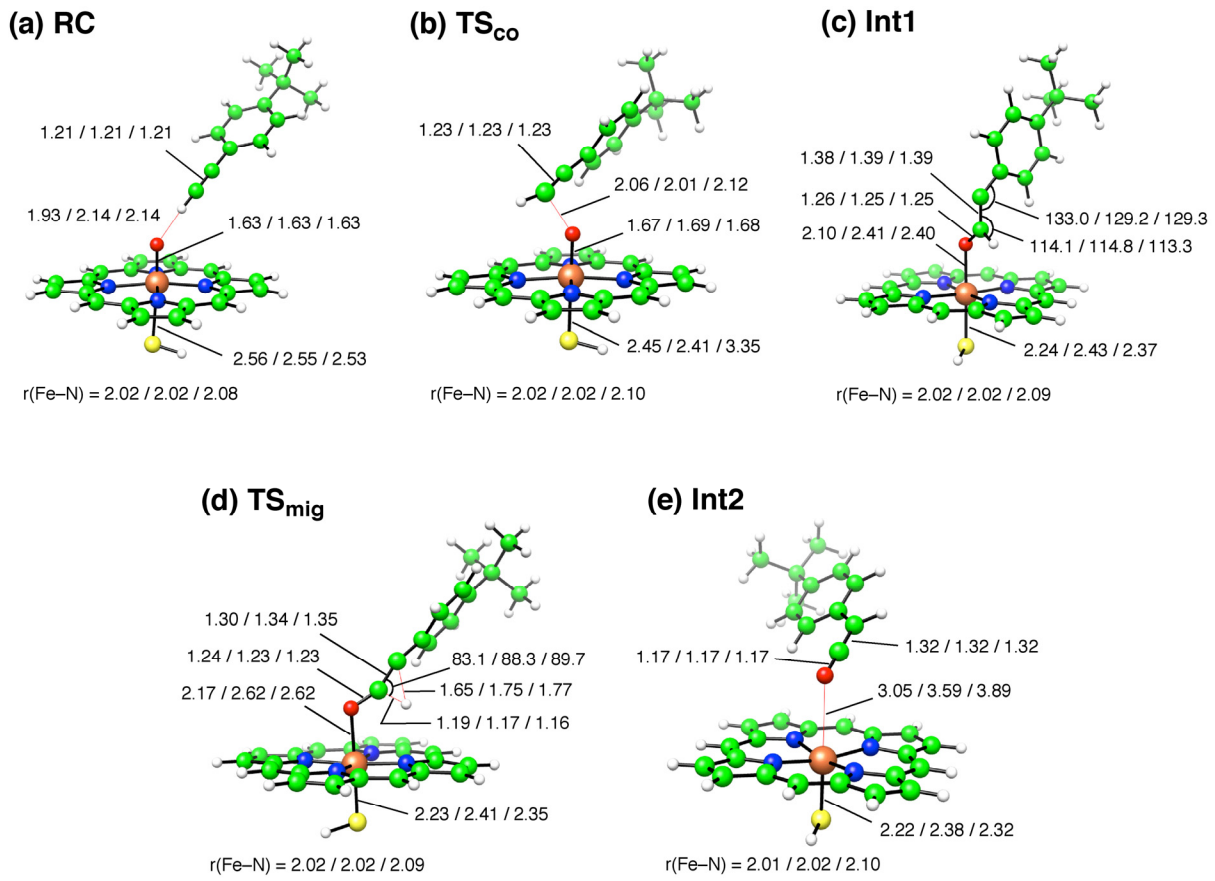

Figure 2. B3LYP/B1-optimized geometries of the key species obtained in the ketene-formation step. Bond distances are in Å and bond angles in degrees. The three values are for the doublet, quartet, and sextet states. The average of the four Fe–N distances, r(Fe–N), is also shown for each species.

In the next step of the reaction, the hydrogen atom at the terminal carbon (C_a) underwent a 1,2-hydride shift to the vicinal internal carbon atom (C_b) of acetylene. The geometries of the transition state for this process, **TS$_{mig}$**, are given in Figure 2d. The H–C_a–C_b angle in **TS$_{mig}$** (83–90°) was somewhat smaller than that observed in **Int1** (113–115°, see Figure 2c), and the C_a–H distance (1.16–1.19 Å) was slightly larger than the standard C–H bond distance at **TS$_{mig}$**. In addition, the Fe–O distance in **TS$_{mig}$** was somewhat larger than that observed for **Int1**, indicating that some amount of electron density in the Fe–O region is being transferred to the C_a–O region to build up a new C=O double bond in the ketene moiety. As can be observed in Figure 1, the barrier for the

1,2-shift was rather small; thus, this step will not have any significant influence on the reaction rate of MBI. This 1,2-shift yields a ketene-type intermediate, **Int2**, in which the Fe–O distance is larger than 3 Å (Figure 2e). Thus, the electrons around the oxygen atom, which were previously used for the interaction with Fe at **Int1**, have totally shifted to the ketene C=O bond. In summary, the highest barrier detected in the ketene formation step (Figure 1) was that of the C_a–O bond formation step (14.1 kcal/mol), which can be surpassed readily. Therefore, the calculations support the conventionally proposed ketene-formation mechanism in MBI by terminal acetylenes.

3.2. Ester bond formation between the ketene and threonine

In the final step of the MBI reaction, the ketene-type metabolic intermediate supposedly reacts with the threonine hydroxyl group, to form an ester bond (Scheme 1). Two possible pathways (Paths A and B) were examined for the reaction between the ketene intermediate (**Int2**) and threonine (see Scheme 3), with the latter modeled by ethanol. This ester bond formation process is assumed to involve nucleophilic attack of the threonine hydroxyl oxygen on the ketene carbon (C_a) and migration of the proton of threonine to the internal carbon (C_b) of the ketene. As a result of this transformation, these two species form a covalent bond, thereby preventing the tBPA substrate from being released from the P450 active site. This conventionally accepted pathway is referred to here as Path A (Scheme 2a). We also examined Path B, which assumes the involvement of a water molecule in the reaction between the ketene and threonine (Scheme 2b). In this pathway, the proton of the threonine hydroxyl group was not directly transferred to the ketene substrate; rather, it was relayed to the catalytic water molecule. Concomitantly, the proton of the water molecule was donated to the internal carbon of the ketene moiety. As a consequence, the ester product and a water molecule were obtained.

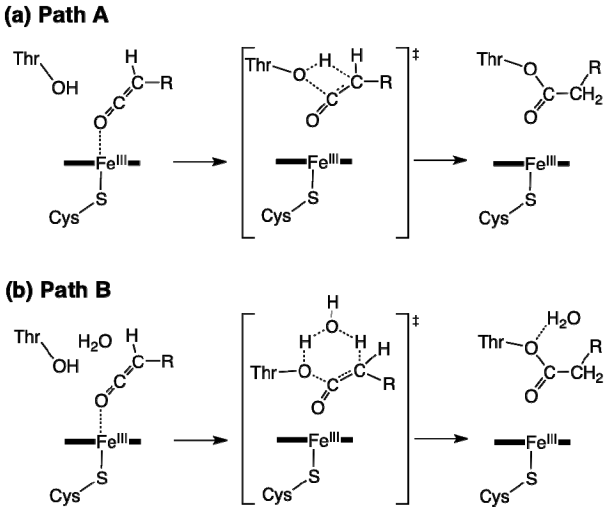

Scheme 3. Two pathways considered for ester bond formation between the ketene and threonine: (a) Path A; (b) Path B.

The energy barriers for ester bond formation in Paths A and B are compared in Figure 3. The reference state for energy calculations was isolated **Int2** and EtOH (i.e., **Int2** + **thr**) for Path A, and isolated **Int2**, EtOH, and H_2O (i.e., **Int2** + **thr** + **w**) for Path B. In Figure 3, the relative energies of the three spin states of these reference states were set as being equal to those of **Int2** in Figure 1. Key optimized geometries on the two esterification pathways are also presented in Figure 4. Over the entire range of the profile, the ground state was calculated to be the sextet state. The profile for Path A is shown on the right-hand side of Figure 3, in which the reaction proceeds from isolated **Int2** + **thr** via a transition state (**TS_{oc}-thr**) to a product (**Pro-thr**). The threonine hydroxyl oxygen attacks the terminal carbon C_a of the ketene and, at the transition state (**TS_{oc}-thr**, Figure 4a), the distance of this forming C_a–O bond is 1.67–1.69 Å. The formation of a C_a–O bond results in dissociation of the threonine hydroxyl hydrogen and its migration to the adjacent carbon of the ketene, to form **Pro-thr**. The reaction barrier for this step in the sextet state was very high (38.2 kcal/mol, see Figure 3), and the other two spin states also exhibited similarly high barrier heights. Hence, Path A involves an unusually high barrier for the formation of an ester bond, which reduces

the likelihood of a role for this mechanism in MBI. In an attempt to seek a more likely reaction mechanism, we placed a water molecule in the vicinity of the reaction center (Scheme 3b). The energy profile of this water-mediated pathway (Path B), for which the reference state is **Int2** + **thr** + **w**, is presented on the left-hand side of Figure 3. We assumed that the isolated fragments are first stabilized upon the formation of a hydrogen bond between the threonine and the water (**Int2** + **thr---w**), and that this stabilized cluster then undergoes the reaction with ketene to form an ester bond. The formation of the hydrogen bond stabilized the system by 1.2–1.3 kcal/mol. In our opinion, the placement of a water molecule at this position is well justifiable in view of the fact that the threonine is located in the proton-relay channel of P450s.[14,27,28] In some of the available X-ray crystal structures of CYP2B4, as deposited at the Protein Data Bank website (PDB codes 1SUO, 1PO5, 2BDM, 3TK3, and 3MVR),[29.30] a water molecule can be found in the vicinity of the threonine residue. Surprisingly, we found that the effect of the water molecule on the reaction was substantial: the transition state (**TS_{oc}-thr-w**, Figure 4b) was significantly stabilized and the reaction barrier in Path B was reduced to 18.5 kcal/mol, which is lower by 19.7 kcal/mol than the unusually high barrier observed in Path A. In the gas-phase calculations at the B3LYP/B1+ZPE(B1) and B3LYP/B2//B1+ZPE(B1) levels, the corresponding barriers were calculated as being 3.7 and 14.3 kcal/mol, respectively. Therefore, the increase in barrier height at the B3LYP(SCRF)/B2//B3LYP/B1+ZPE(B1) level (18.5 kcal/mol) was attributed largely to a basis-set effect that originated from the inadequacy of B1 in describing the transition state (**TSoc-thr-w**) in which a few partially anionic species are involved, and partly to the solvent effect. To assess the heme Lewis-acid effect on this esterification step in Path B, we also performed geometry optimization calculations after removing the heme-SH moiety (Figure S2). The calculated barrier for this purely organic reaction was 19.9 kcal/mol for Path B, which means that the decrease in the barrier in the presence of the heme-SH moiety was only 1.4 kcal/mol. Thus, the Lewis-acid effect

on this step was fairly small. Our results strongly support the hypothesis that a water molecule is involved in the reaction between ketene and threonine. Upon completion of the reaction, a complex of an ester product and a water molecule (**Pro-thr-w**) was obtained, in which a water molecule formed a hydrogen bond with the ester product (Figure 4b).

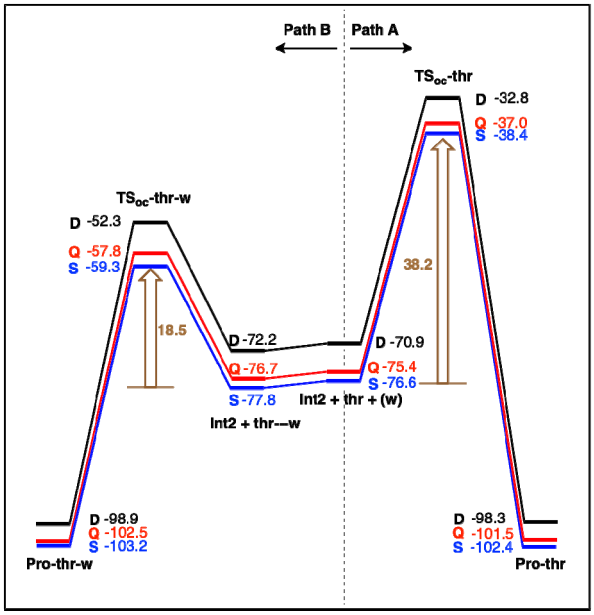

Figure 3. Energy profiles of the ester bond formation step, as obtained at the B3LYP(SCRF)/B2//B3LYP/B1+ZPE(B1) level. The black, red and blue lines indicate the energy changes for the doublet (**D**), quartet (**Q**), and sextet (**S**) states, respectively. The profiles for Paths A and B are shown in the right- and left-hand panels, respectively. The relative energies are given in kcal/mol.

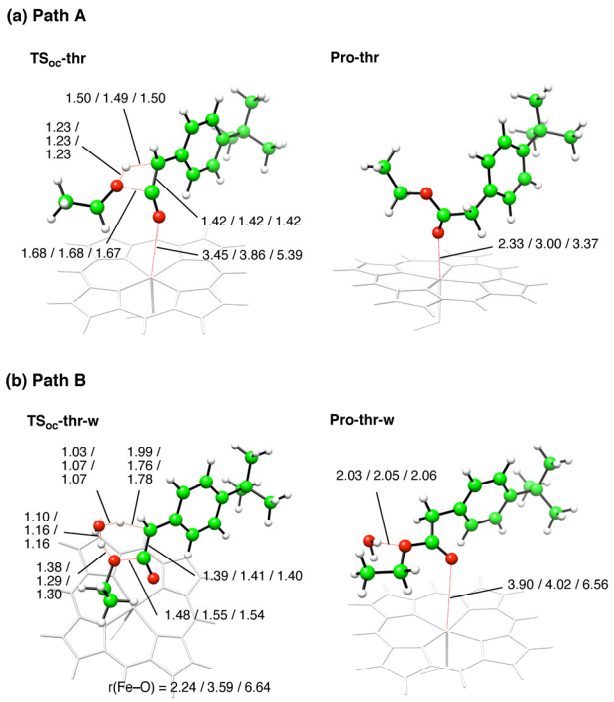

Figure 4. B3LYP/B1-optimized geometries of the esterification transition states and products in Paths A and B. Bond distances are in Å and bond angles in degrees. The three values are for the doublet, quartet, and sextet states.

The reaction-energy diagram (Figure 1) suggests that at the **Int2** stage, the sextet state was the ground state and that the reaction between the ketene intermediate and threonine proceeded with the heme moiety remaining in a sextet ferric state. It should be mentioned that when the ferric state has a sixth water ligand at the distal coordination site, the low-spin (doublet) state is preferred.[10b,12] Although a detailed examination of this water ligand is outside the scope of this study, our model envisages that if the ketene-threonine reaction takes place in the proximity of the iron center, the water coordination to Fe would be hindered during the reaction, resulting in high-spin reactivity. However, if the reaction is preceded by a large movement of the ketene, then water coordination to Fe is permitted and low-spin reactivity would be preferred. The relatively long Fe–O distances in the optimized geometries of the products (**Pro-thr** or **Pro-thr-w**) suggest that the product cannot coordinate strongly to iron. Thus, the distal site of the iron would be easily vacated, which would

allow the coordination of a nearby water molecule at the iron center. It is interesting to note that in the X-ray structure of CYP2B4 bound to tBPA (PDB code 3R1A),[10a] a water molecule is present just over the Fe ion. This may be the water molecule that has catalyzed the reaction (Scheme 3b) and has migrated from the reaction site to Fe after the reaction.

It is also interesting to note that the MBI reaction considered here was highly exothermic, with the final product (**Pro-thr** or **Pro-thr-w**) being > 100 kcal/mol more stable than the initial **RC** state. In contrast, in P450 hydroxylation and epoxidation reactions, the energy of product complexes was only around 40–50 kcal/mol lower than that of the initial state.[16] The large exothermicity of the tBPA reaction implies the remarkable stability of the covalent adduct, which would prevent its release from the P450 active site.

3.3. N-alkylation of prosthetic heme.

So far we have discussed a specific type of reaction between tBPA and P450 Cpd I in which the terminal carbon atom (C_a) of acetylene forms a covalent bond with the oxo unit of Cpd I. This leads to ketene formation, followed by protein modification at Thr302 (Scheme 1). Another known pathway for MBI by acetylene compounds is the alkylation of the P450 prosthetic heme at an equatorial nitrogen atom (Scheme 4).[2,3,31] This N-alkylation reaction requires the initial attack of Cpd I oxoiron(IV) on the vicinal internal carbon (C_b), rather than on C_a. Although tBPA undergoes the former threonine-esterification reaction, several other acetylene compounds undergo N-alkylation. Therefore, it is fundamentally interesting to assess the N-alkylation pathway in the case of tBPA.

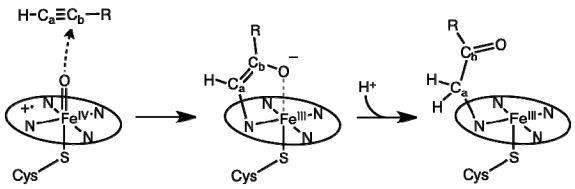

Scheme 4. Likely mechanism of heme N-alkylation by acetylene compounds.

Figure 5 shows the calculated energy profile for the N-alkylation pathway, whereas Figure 6 shows the optimized geometries of key species. The starting point, **RC**, was the same as that used in the ketene-formation pathway (Figure 1). In the N-alkylation pathway, however, the oxo unit of Cpd I attacked the internal carbon (C_b). This resulted in the formation of a C_b–O bond via the transition state **$TS_{co}(C_b)$**. As can be seen in Figure 5, the doublet state was the most favorable spin state for this C_b–O bond formation, and its barrier was calculated as 22.2 kcal/mol. This energy barrier was somewhat higher than that observed for ketene formation (14.1 kcal/mol, see Figure 1). Furthermore, Figure 6a shows that the C–O distance in the forming C_b–O bond at **$TS_{co}(C_b)$** was slightly shorter (1.93–2.02 Å) than that observed in the ketene-formation pathway (2.01–2.12 Å, Figure 2), implying a late transition state in the N-alkylation reaction. Thus, calculations showed that the attack of oxoiron(IV) on the internal carbon of acetylene is not as favorable as that on the terminal carbon. The calculated preference for C_a–O bond formation is consistent with the experimental observation that tBPA gives covalent modification of threonine.[10] In the doublet state, C_b–O bond formation led directly to the N-alkylated intermediate **Int2(C_b)**. However, before the formation of **Int2(C_b)**, the quartet and sextet reaction pathways involved the intermediate **Int1(C_b)**, in which the formation of the C_b–O bond was completed without formation of a C_a–N bond (Figure 6b). In the sextet state, the subsequent C_a–N bond formation by **Int1(C_b)** was rather facile, as it required only radical coupling between C_a and N in the oxidized porphyrin ligand. In the sextet state, at the B3LYP(SCRF)/B2//B3LYP/B1+ZPE(B1) level, the formation of the C_a–N bond via

$TS_{cn}(C_b)$ had a barrier of only 2.7 kcal/mol (Figure 5) and the C_a–N distance at **$TS_{cn}(C_b)$** was fairly long (3.33 Å, Figure 6c). In contrast, the quartet **Int1(C_b)** possessed an unusual electronic state involving formal Fe(V) and two unpaired spin-up electrons on the C_a atom; in addition, the C_a–N distance at **$TS_{cn}(C_b)$** was shorter (1.93 Å). Its electron reorganization to form **Int2(C_b)**, which has both a C_a–N bond and a C_b–O bond (Figure 5d), required a reaction barrier of 16.7 kcal/mol and **Int2(C_b)** was relatively unstable because of the π-anionic character of the porphine ligand. A more stable **Int2(C_b)** state (**Int2(C_b)'**) with a normal Fe(III) electron configuration was found in the quartet state; however, this state originated in an unstable intermediate **Int1(C_b)'**. The comparison of all energy data obtained suggests that the doublet state is the most favorable spin state for the formation of **Int2(C_b)**. The C_a atom of **Int2(C_b)** will accept an additional proton to form a final alkylated product (Scheme 4).

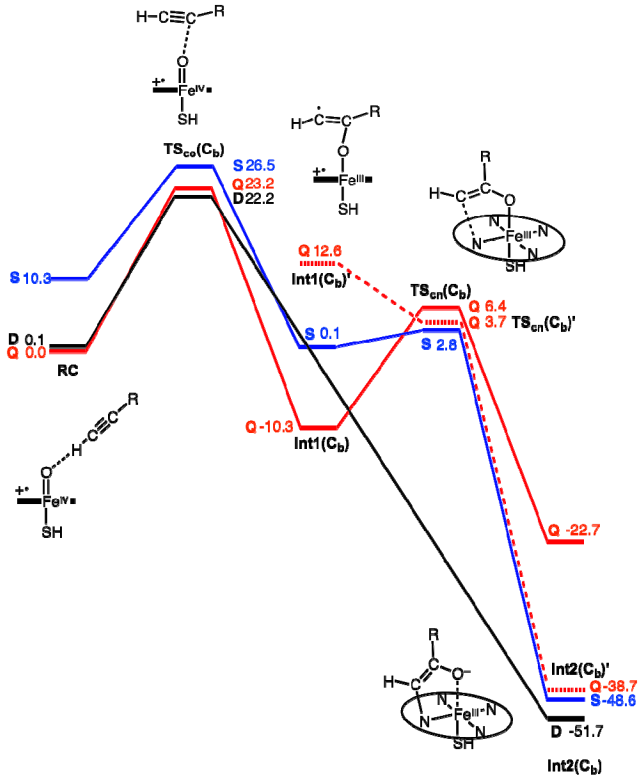

Figure 5. DFT calculated reaction energy profile for N-alkylation, as obtained at the

B3LYP(SCRF)/B2//B3LYP/B1+ZPE(B1) level. The black, red and blue lines indicate the energy changes for the doublet (**D**), quartet (**Q**), and sextet (**S**) states, respectively. Relative energies are given in kcal/mol.

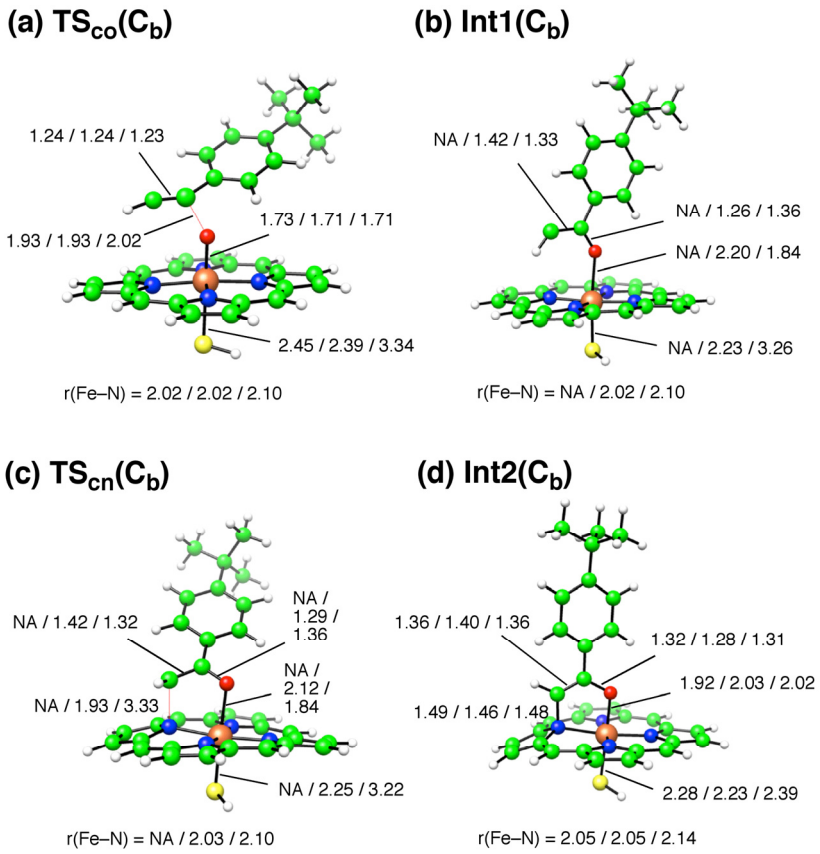

Figure 6. Optimized geometries of the transition states and products in the N-alkylation pathway. Bond distances are in Å and bond angles in degrees. The three values are for the doublet, quartet, and sextet states.

4. Conclusion

We performed DFT calculations to study the atomistic details of the MBI of cytochrome P450 by tBPA. The pathway leading to protein modification at a nearby threonine residue was initiated by the formation of a covalent bond between the terminal carbon and the oxo moiety of P450 Cpd I. This C–O bond formation step was rather facile, and was followed by a 1,2-hydride shift to form a

ketene intermediate. The barrier for the reaction between the ketene intermediate and the threonine residue was too high in the absence of a water catalyst. Interestingly, a water catalyst lowered the reaction barrier substantially; therefore, we propose that a water molecule renders the MBI of CYP2B4 by tBPA feasible. A key message derived from our computational study is, therefore, that a single water molecule can regulate the fate of an enzyme. Another possible MBI mode involves the initial formation of a covalent bond between the internal carbon of acetylene and Cpd I, which eventually alkylates the heme prosthetic group. However, this MBI pathway was calculated to be less favorable.

Future studies using DFT/MM calculations will provide a more accurate view of MBI, especially of the effect of the protein environment and the role of a water molecule as a ligand or a catalyst. There has been an increase in the use of a variety of *in silico* tools to further the understanding of P450 metabolism.[32] To date, quantum-chemistry-based methods have not been major tools in this setting because of their high computational demand. However, in view of their ability to describe chemical reactions, namely the essential part of MBI, in the coming decades, DFT and DFT/MM calculations will play active roles in this line of research. A detailed understanding of MBI using quantum chemistry should be an important step toward the establishment of strategies for the prediction of metabolism and the design of new mechanism-based inactivators.

Acknowledgment

This work was supported by a Nanyang Assistant Professorship. We thank the High Performance Computing Centre at Nanyang Technological University for computer resources.

Supporting Information Available: Complete Ref 20, raw energy data, Mulliken group spin

densities and group charges for optimized geometries, geometries of all optimized geometries, and XYZ coordinates of optimized geometries. This material is available free of charge via the Internet at http://pubs.acs.org.

References

1 Silverman, R. B. *Methods Enzymol.* **1995**, *249*, 240-283.

2 Ortiz de Montellano, P. R.; Correia, M. A. *Cytochrome P450: Structure, Mechanism, and Biochemistry*, 3rd ed.; Kluwer Academic/Plenum Press: New York, 2005; pp 247-322.

3 (a) Kent, U. M.; Jushchyshyn, M. I.; Hollenberg, P. F. *Curr. Drug. Metab.* **2001**, *2*, 215-243. (b) Hollenberg, P. F.; Kent U. M.; Bumpus, N. N. *Chem. Res. Toxicol.* **2008**, *21*, 189-205.

4 Halpert, J. R. *Annu. Rev. Pharmacol. Toxicol.* **1995**, *35*, 29-53.

5 Blobaum, A. L. *Drug Metab. Dispos.* **2006**, *34*, 1-7.

6 Venkatakrishnan, K.; von Moltke, L. L.; Greenblatt, D. J. *J. Clin. Pharmacol.* **2001**, *41*, 1149-1179.

7 Guengerich, F. P. *Chem. Res. Toxicol.* **1990**, *3*, 363-371.

8 Obach, R. S.; Walsky, R. L.; Venkatakrishnan, K. *Drug Metab. Dispos.* **2007**, *35*, 246-255.

9 Zhou, S.; Chan, S. Y.; Goh, B. C.; Chan, E.; Duan, W.; Huang M.; McLeod, H. L. *Clin. Pharmacokinet.* **2005**, *44*, 279-304.

10 (a) Gay, S. C.; Zhang, H.; Wilderman, P. R.; Roberts, A. G.; Liu, T.; Li, S.; Lin, H.; Zhang, Q.; Woods, V. L., Jr.; Stout, C. D., et al. *Biochemistry* **2011**, *50*, 4903-4911. (b) Zhang, H.; Lin, H.; Walker, V. J.; Hamdane, D.; Hollenberg, P. F. *Mol. Pharmacol.* **2009**, *76*, 1011-1018. (c) Lin, H.; Zhang, H.; Jushchyshyn, M.; Hollenberg, P. F. *J. Pharmacol. Exp.*

Ther. **2010**, *333*, 663-669. (d) Lin, H.; Zhang, H.; Pratt-Hyatt, M. J.; Hollenberg, P. F. *Drug Metab. Dispos.* **2011**, *39*, 2431-2439. (e) Zhang, H.; Lin, H.; Kenaan, C.; Hollenberg, P. F. *Arch. Biochem. Biophys,* **2011**, *507*, 135-143.

11 (a) Chan, W. K.; Sui, Z.; Ortiz de Montellano, P. R. *Chem. Res. Toxicol.* **1993**, *6*, 38-45. (b) Regal, K. A.; Schrag, M. L.; Kent, U. M.; Wienkers, L. C.; Hollenberg, P. F. *Chem. Res. Toxicol.* **2000**, *13*, 262-270.

12 Mak, P. J.; Zhang, H.; Hollenberg, P. F.; Kincaid, J. R. *J. Am. Chem. Soc.* **2010**, *132*, 1494-1495.

13 Denisov, I. G.; Makris, T. M.; Sligar, S. G.; Schlichting, I. *Chem. Rev.* **2005**, *105*, 2253–2277.

14 (a) Meunier, B.; de Visser, S. P.; Shaik, S. *Chem. Rev.* **2004**, *104*, 3947-3980. (b) Shaik, S.; Kumar, D.; de Visser, S. P.; Altun, A.; Thiel, W. *Chem. Rev.* **2005**, *105*, 2279-2328. (c) Shaik, S.; Cohen, S.; Wang, Y.; Chen, H.; Kumar, D.; Thiel, W. *Chem. Rev.* **2010**, *110*, 949-1017.

15 (a) Shaik, S.; Hirao, H.; Kumar, D. *Acc. Chem. Res.* **2007**, *40*, 532-542. (b) Shaik, S.; Hirao, H.; Kumar, D. *Nat. Prod. Rep.* **2007**, *24*, 533-552.

16 Hirao, H.; Kumar, D.; Thiel, W.; Shaik, S. *J. Am. Chem. Soc.* **2005**, *127*, 13007-13018.

17 Kamachi, T.; Yoshizawa, K. *J. Am. Chem. Soc.* **2003**, *125*, 4652-4661.

18 Lonsdale, R.; Harvey, J. N.; Mulholland, A. J. *Chem. Soc. Rev.* **2012**, *41*, 3024-3038.

19 Guallar, V.; Gherman, B. F.; Lippard, S. J.; Friesner, R. A. *Curr. Opin. Chem. Biol.* **2002**, *6*, 236-242.

20 Frisch, M. J.; Trucks, G. W.; Schlegel, H. B.; Scuseria, G. E.; Robb, M. A.; Cheeseman, J. R.; Scalmani, G.; Barone, V.; Mennucci, B.; Petersson, G. A., et al. Gaussian 09, Revision B.01; Gaussian, Inc.: Wallingford, CT, 2010.

21 (a) Becke, A. D. *J. Chem. Phys.* **1993**, *98*, 5648-5652. (b) Lee, C.; Yang, W.; Parr, R. G. *Phys. Rev. B* **1988**, *37*, 785-789. (c) Vosko, S. H.; Wilk, L.; Nusair, M. *Can. J. Phys.* **1980**, *58*, 1200-1211.

22 (a) Dolg, M.; Wedig, U.; Stoll, H.; Preuss, H. *J. Chem. Phys.* **1987**, *86*, 866-872. (b) Hehre, W.; Radom, L.; Schleyer, P. v. R.; Pople, J. *Ab Initio Molecular Orbital Theory*, John Wiley & Sons: New York, 1986.

23 Cancès, M. T.; Mennucci, B.; Tomasi, J. *J. Chem. Phys.* **1997**, *107*, 3032-3041.

24 Ogliaro, F.; Cohen, S.; de Visser, S. P.; Shaik, S. *J. Am. Chem. Soc.* **2000**, *122*, 12892-12893

25 Pettersen, E. F.; Goddard, T. D.; Huang, C. C.; Couch, G. S.; Greenblatt, D. M.; Meng E. C.; Ferrin, T. E. *J. Comput. Chem.* **2004**, *25*, 1605-1612.

26 Fukui, K. *Acc. Chem. Res.* **1981**, *14*, 363-368.

27 Nagano, S.; Poulos, T. L. *J. Biol. Chem.* **2005**, *280*, 31659-31663.

28 (a) Kamachi, T.; Yoshizawa, K. *J. Am. Chem. Soc.* **2003**, 125, 4652. (b) Kumar, D.; Hirao, H.; de Visser, S. P,; Zheng, J. J. Wang, D. Q. Thiel, W.; Shaik, S. *J. Phys. Chem. B* **2005**, *109*, 19946-19951. (c) Zheng, J. J. Wang, D. Q. Thiel, W.; Shaik, S. *J. Am. Chem. Soc.* **2006**, *128*, 13204-13215.

29 Protein Data Bank (PDB). http://www.rcsb.org (accessed Apr 12, 2012).

30 (a) Scott, E. E.; White, M. A.; He, Y. A.; Johnson, E. F.; Stout, C. D.; Halpert, J. R. *J. Biol. Chem.* **2004**, *279*, 27294-27301. (b) Scott, E. E.; He, Y. A.; Wester, M. R.; White, M. A.; Chin, C. C.; Halpert, J. R.; Johnson, E. F.; Stout, C. D. *Proc. Natl. Acad. Sci. USA* **2003**, *100*, 13196-13201. (c) Zhao, Y.; White, M. A.; Muralidhara, B. K.; Sun, L.; Halpert, J. R.; Stout, C. D. *J. Biol. Chem.* **2006**, *281*, 5973-5981. (d) Wilderman, P. R.; Shah, M. B.; Liu, T.; Li, S.; Hsu, S.; Roberts, A. G.; Goodlett, D. R.; Zhang, Q.; Woods, V. L.; Stout, C.

D.; Halpert, J. R. *J. Biol. Chem.* **2010**, *285*, 38602-38611.

31 Ortiz de Montellano, P. R.; Kunze, K. L. *J. Biol. Chem.* **1980**, *255*, 5578-5585.

32 Sun, H.; Scott, D. O. *Chem. Biol. Drug. Des.* **2010**, *75*, 3-17.

TOC

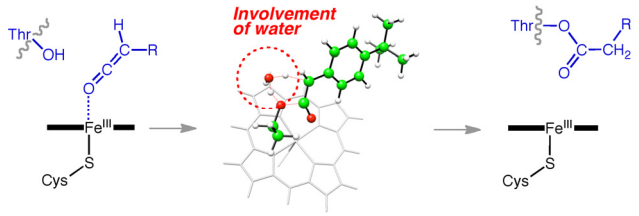

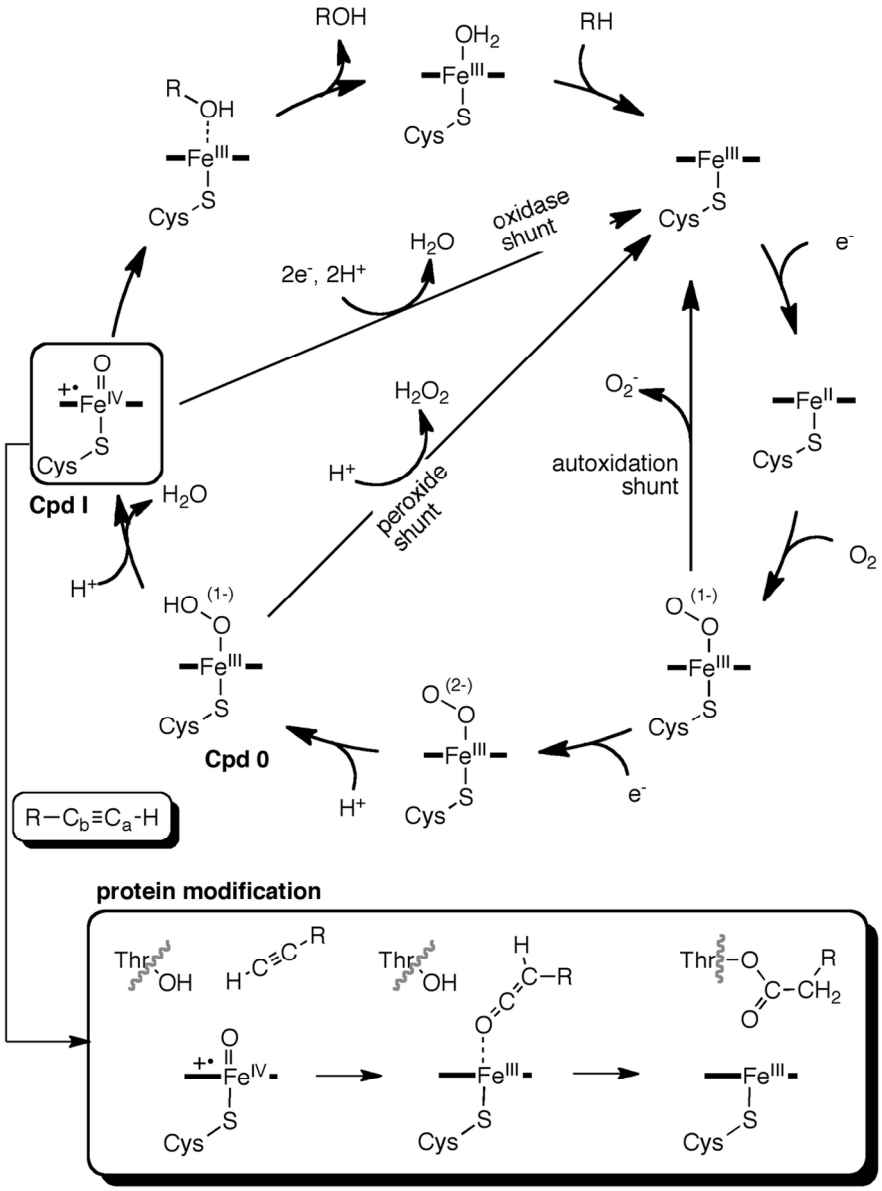

Scheme 1
108x146mm (300 x 300 DPI)

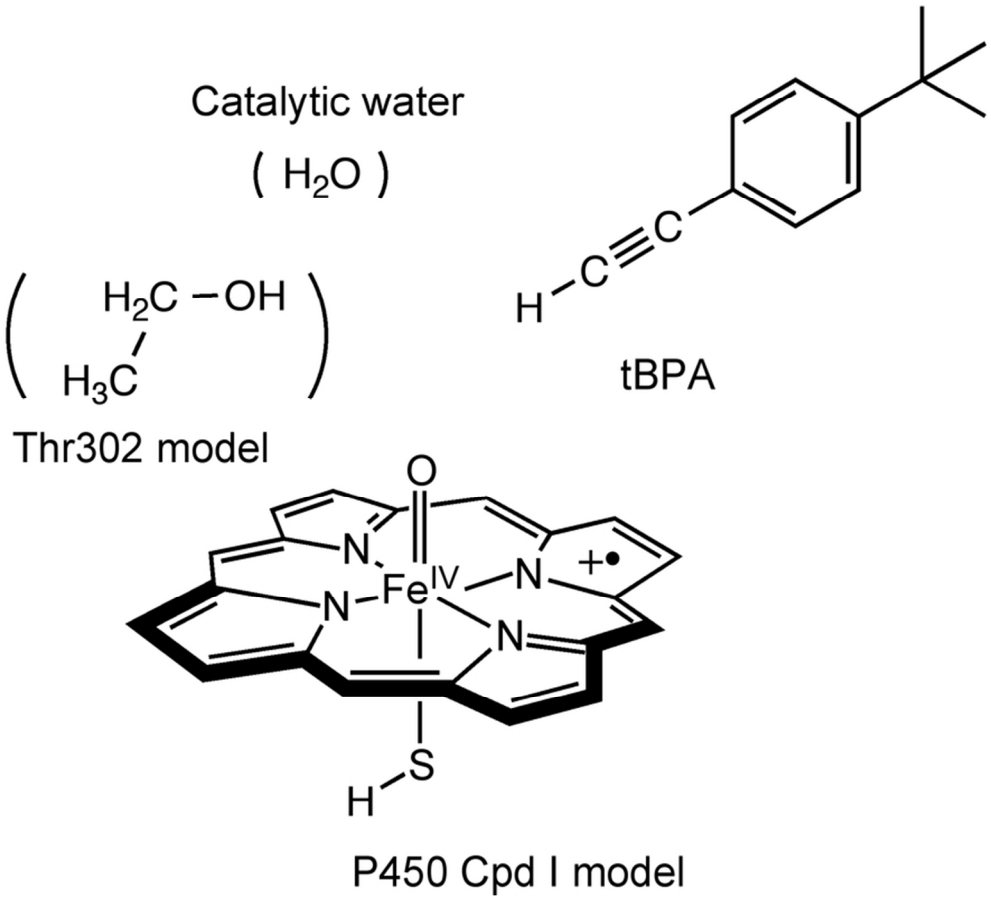

Scheme 2
75x67mm (300 x 300 DPI)

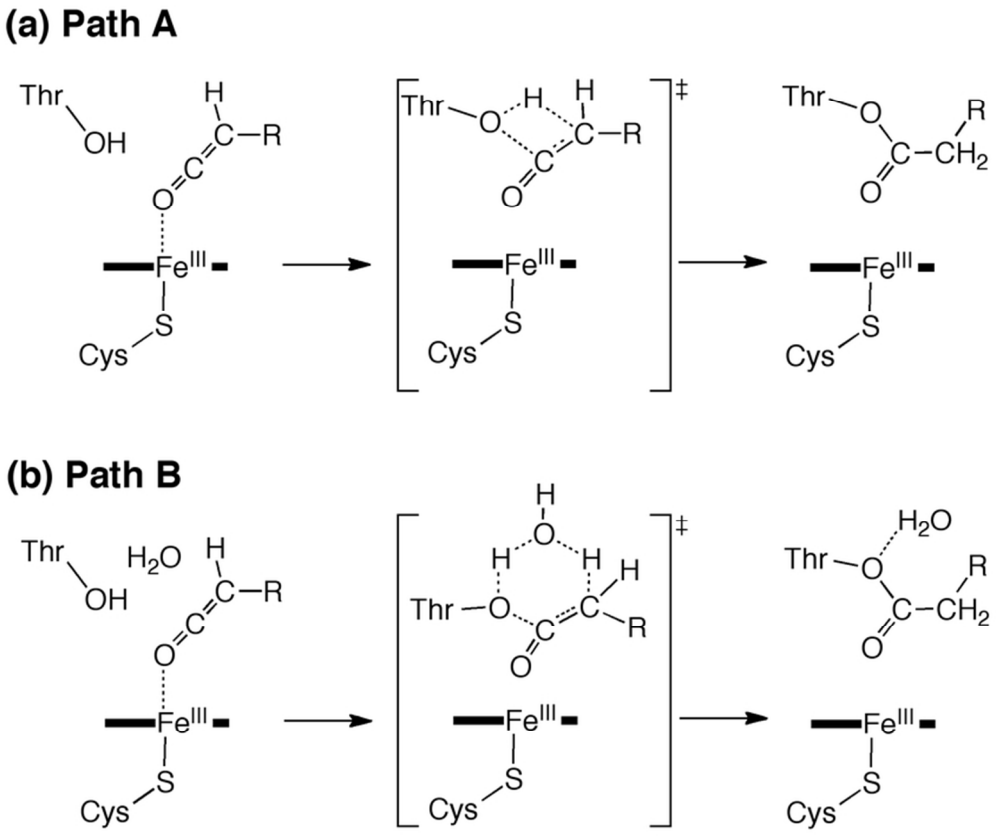

Scheme 3
71x60mm (300 x 300 DPI)

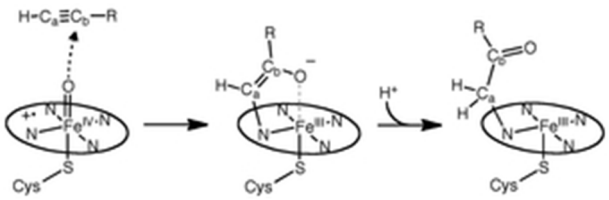

Scheme 4
25x8mm (300 x 300 DPI)

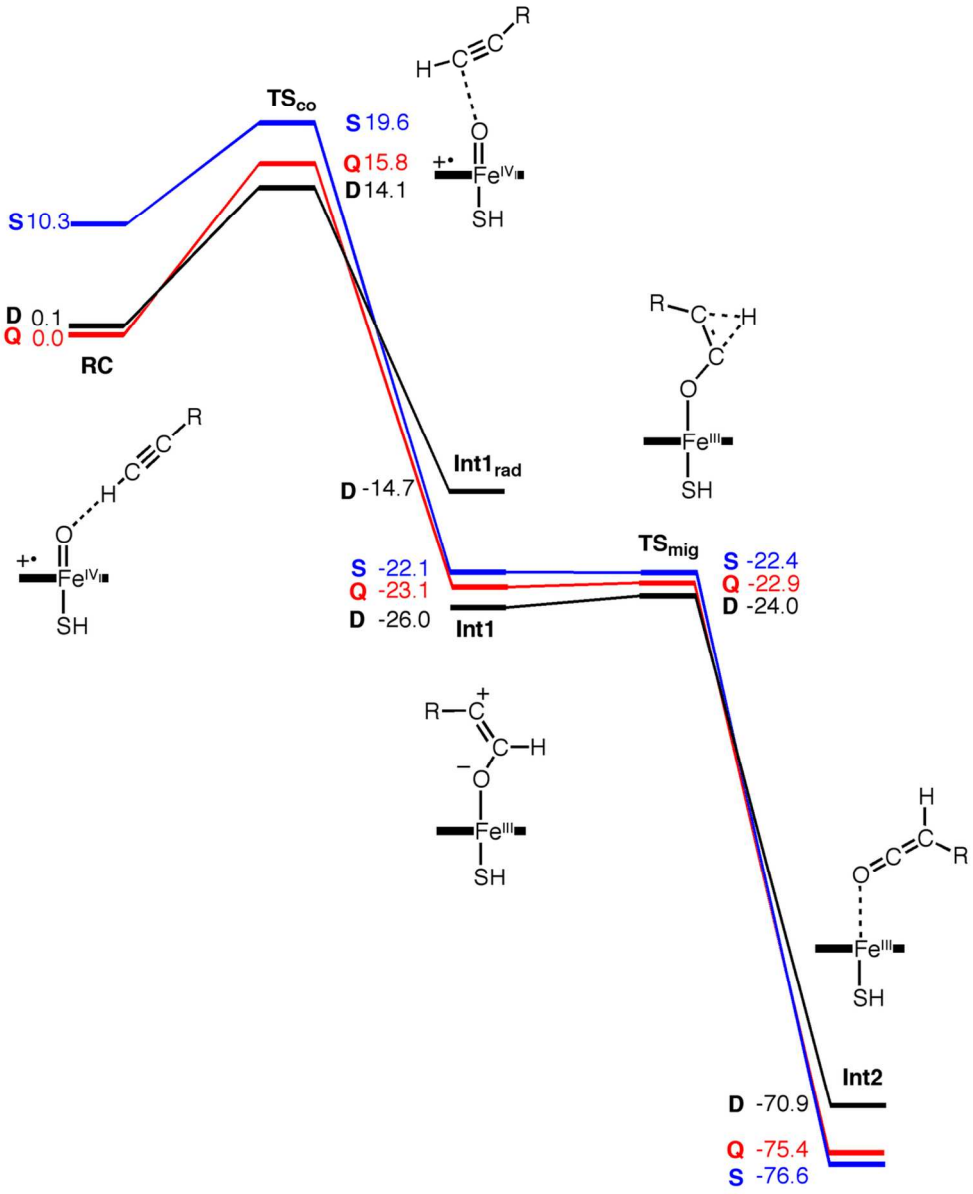

Figure 1
110x135mm (300 x 300 DPI)

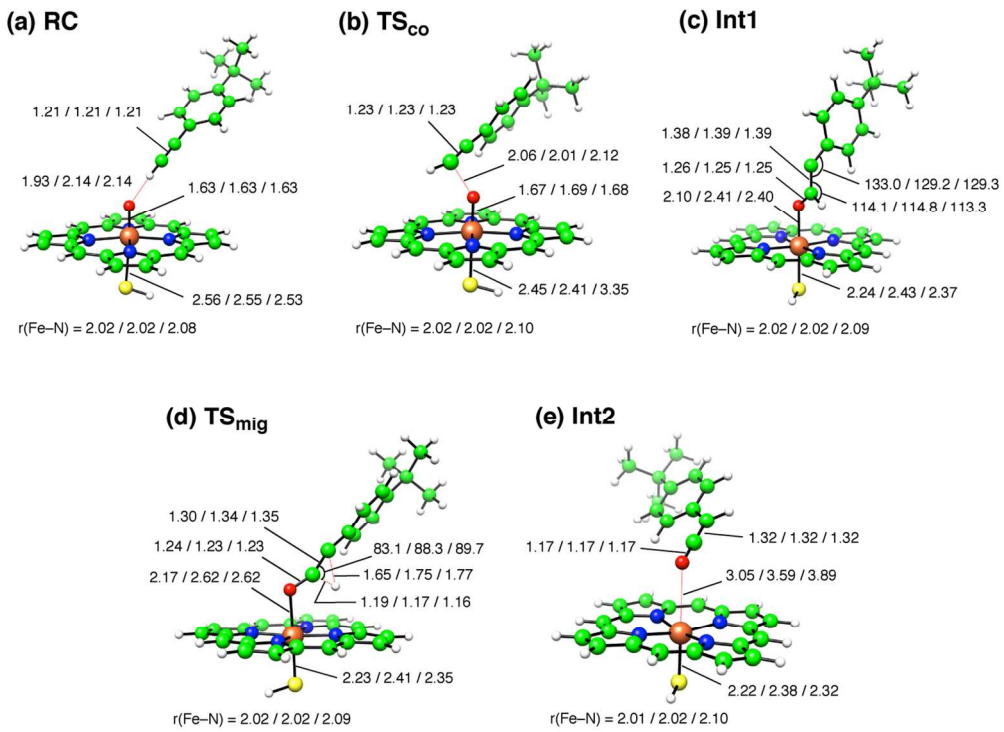

Figure 2
125x90mm (300 x 300 DPI)

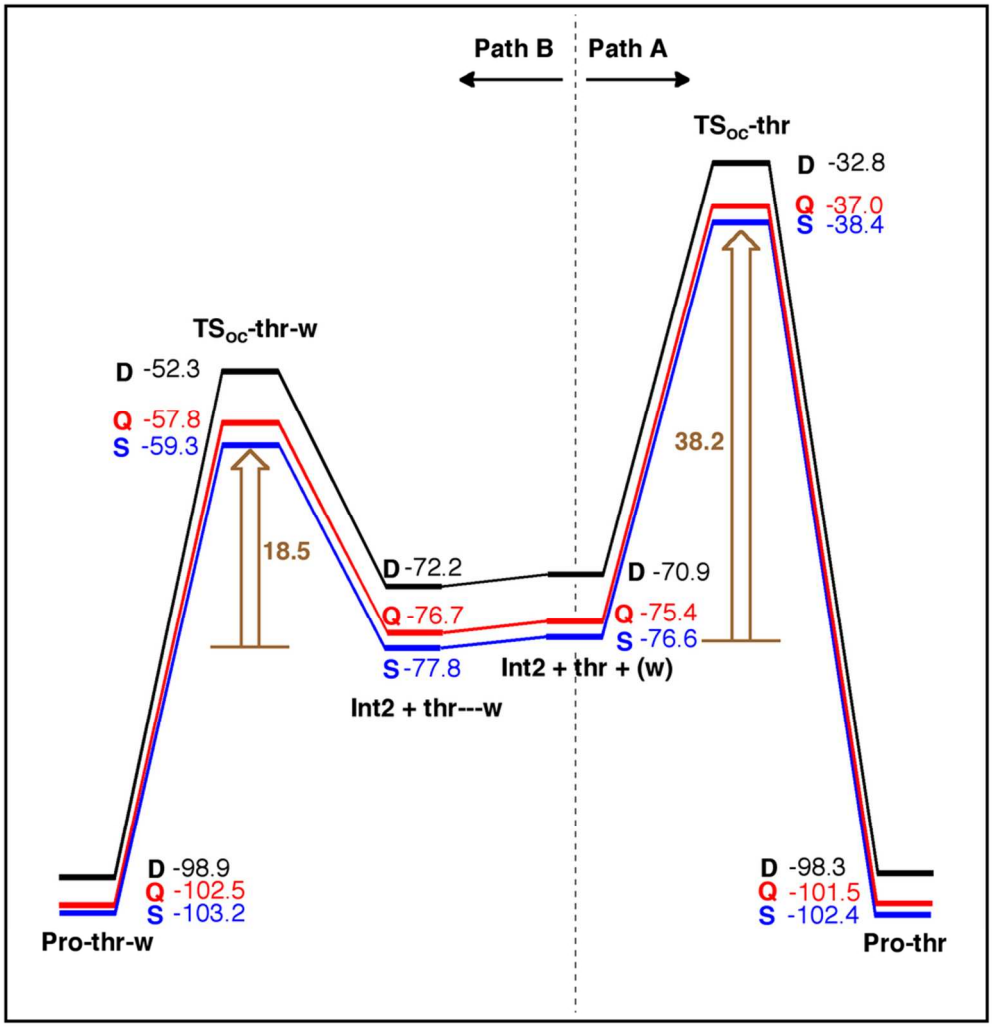

Figure 3
86x89mm (300 x 300 DPI)

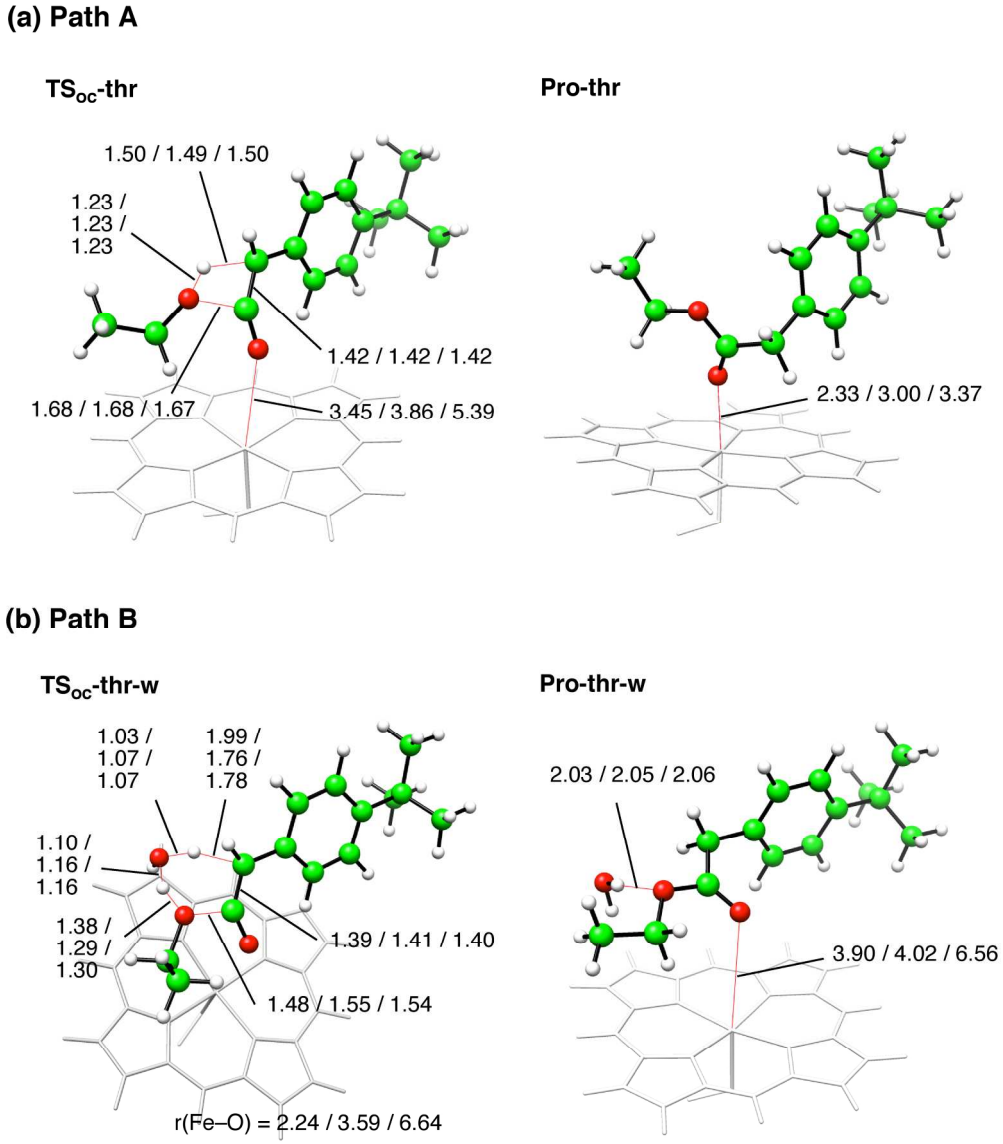

Figure 4
202x233mm (300 x 300 DPI)

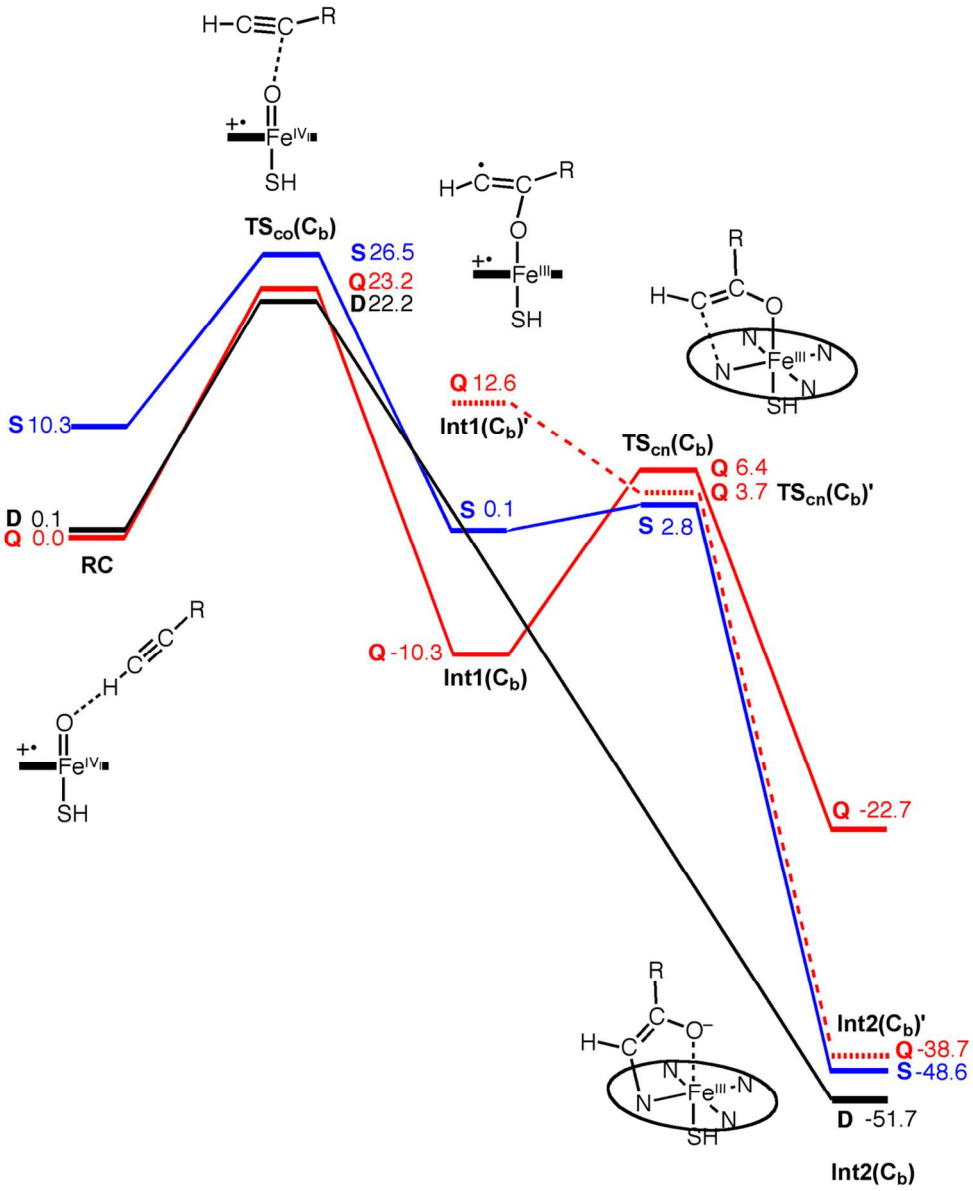

Figure 5
110x134mm (300 x 300 DPI)

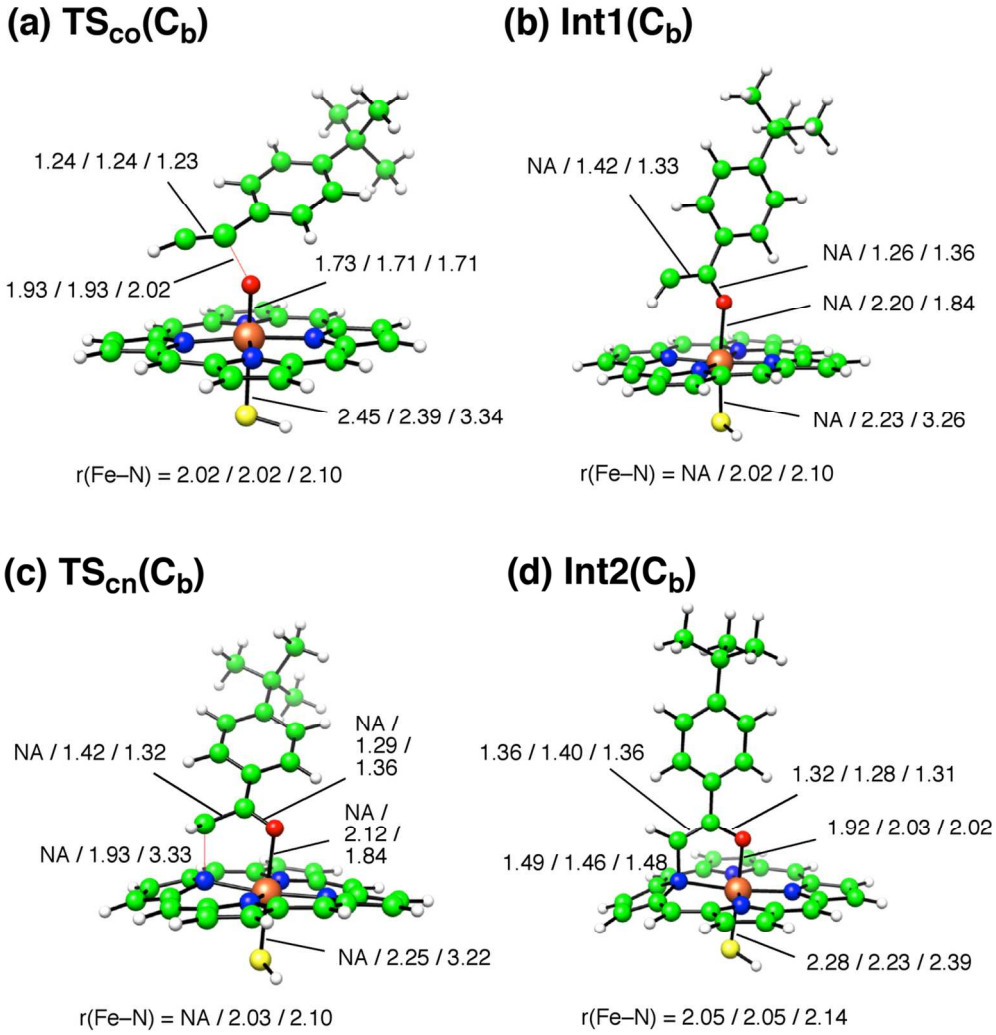

Figure 6
119x124mm (300 x 300 DPI)

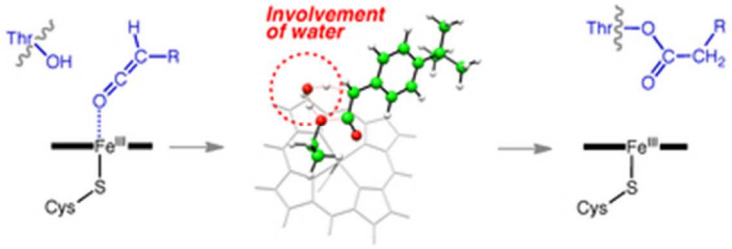

TOC graphic
30x10mm (300 x 300 DPI)